Longitudinal association between magnetotail reconnection and auroral breakup based on Geotail and Polar observations

A. Ieda,[1] D. H. Fairfield,[2] J. A. Slavin,[2] K. Liou,[3] C.-I. Meng,[3] S. Machida,[4] Y. Miyashita,[5] T. Mukai,[5] Y. Saito,[5] M. Nosé,[6] J.-H. Shue,[7] G. K. Parks,[8] and M. O. Fillingim[8]

Received 26 February 2008; revised 12 March 2008; accepted 28 March 2008; published 6 August 2008.

[1] The dawn–dusk locations of reconnection in the near-earth magnetotail at the time of isolated auroral breakup are studied to clarify whether breakup is always accompanied by reconnection. The near-earth reconnection is identified by tailward plasma flows faster than 200 km/s with southward magnetic field. We first identified 66 breakups in the Polar ultraviolet imager observations of the nightside polar ionosphere. We then studied tailward flows during breakups using Geotail in situ observations of the plasma sheet between 25 and 31 R_E down the tail. It was found that the dawn–dusk (Y) locations of relatively fast ($\geq$400 km/s) tailward flows were associated with breakup magnetic local time (MLT) by a regression line of $Y_{AGSM} = -5.7 \times (MLT + 0.6)\ R_E$ with a correlation coefficient of 0.8. Most tailward flows were observed within 5 R_E of the modeled Y locations, where tailward flows occurred in 88% of the 26 cases of breakups between 22 and 0 MLT. It is thus inferred that in most cases, breakup is accompanied by tailward flow near the breakup MLT with its dawn–dusk dimension $\sim$10 R_E. There were only two events without tailward flows in the region where flows have been expected. These two events were an earthward flow event and a traveling compression region event, which are not inconsistent with the initiation of the near-earth reconnection. Auroral breakup is thus likely to always be accompanied by near-earth reconnection near breakup MLT. It is also inferred that reconnection and breakup occur simultaneously within a few minutes, assuming a time delay between reconnection onset and the arrival of tailward flows at satellite locations.

Citation: Ieda, A., et al. (2008), Longitudinal association between magnetotail reconnection and auroral breakup based on Geotail and Polar observations, *J. Geophys. Res.*, *113*, A08207, doi:10.1029/2008JA013127.

1. Introduction

[2] Reconnection in the near-earth magnetotail is one of the most plausible mechanisms to cause auroral breakups in the polar ionosphere [e.g., *Baker et al.*, 1996]. Early studies suggested a close association between near-earth reconnection as identified by tailward flows in the distant tail beyond $\sim$60 R_E and auroral breakup as identified by ground magnetic field variations [*Moldwin and Hughes*, 1993; *Slavin et al.*, 1993; *Nagai et al.*, 1994]. However, even fully developed reconnection does not always correspond to full-fledged breakups but only to spatially localized auroral brightenings [*Ieda et al.*, 2001; *Ohtani et al.*, 2002]. The relationship between reconnection and breakup is thus still not completely clear.

[3] *Nagai et al.* [1998] studied fast flows in the near-earth magnetotail around the time of the auroral breakup as identified by ground magnetic field variations. They found a statistically recognizable global flow pattern within 10 min of breakup. This pattern showed earthward flows earthward of 20–30 R_E down the tail and tailward flows beyond this location, suggesting that reconnection tends to occur between 20 and 30 R_E during breakup. Such global flow patterns were also suggested to develop around the times of breakups [i.e., *Machida et al.*, 1999, 2000; *Miyashita et al.*, 2003]. In contrast, *Lui et al.* [1998] found no such statisti-

[1]Solar-Terrestrial Environment Laboratory, Nagoya University, Nagoya, Aichi, Japan.
[2]Heliophysics Science Division, NASA Goddard Space Flight Center, Greenbelt, Maryland, USA.
[3]Applied Physics Laboratory, Johns Hopkins University, Laurel, Maryland, USA.
[4]Department of Geophysics, Kyoto University, Kyoto, Japan.
[5]Institute of Space and Astronautical Science, Japan Aerospace Exploration Agency, Sagamihara, Kanagawa, Japan.
[6]Data Analysis Center for Geomagnetism and Space Magnetism, Graduate School of Science, Kyoto University, Kyoto, Japan.
[7]Institute of Space Science, National Central University, Jhongli, Taiwan.
[8]Space Sciences Laboratory, University of California, Berkeley, California, USA.

Copyright 2008 by the American Geophysical Union.
0148-0227/08/2008JA013127

cally significant global flow pattern and emphasized that fast flows were rarely observed at breakups.

[4] These previous studies appear to indicate that at least some breakup events involve reconnection, but fast flows are too rarely observed to readily conclude that breakup is always associated with reconnection. The rarity of such fast flows may thus suggest that reconnection is not a necessary condition for breakup. It is also possible that the rarity of fast flows is due to localization of the flows, resulting in lower apparent occurrence rates, even though all breakups may involve reconnection.

[5] The purpose of this study is to clarify whether breakup is always accompanied by near-earth reconnection. The occurrence rate of reconnection was estimated in this study after requiring that the Geotail be located in a favorable region to observe localized flows if they occur. Only breakup events for which Geotail was in the central plasma sheet prior to breakup were considered. Breakup longitude was also considered in order to ensure that Geotail was at a presumably appropriate longitude to observe flows.

[6] Tailward flows with southward magnetic field were employed in this study to indicate the occurrence of near-earth reconnection during auroral breakup. It is believed that magnetic reconnection in the magnetotail occurs at two different radial distances from the earth: the near-earth neutral line (NENL) at 20–30 R_E and the distant neutral line (DNL) at ~100 R_E down the tail [*Slavin et al.*, 1985; *Nishida et al.*, 1996]. Reconnection either at NENL or DNL yields a pair of flows with opposite magnetic polarity: an earthward flow with northward magnetic field, and a tailward flow with southward magnetic field.

[7] Previous statistical studies have actually found that earthward and tailward fast flows are often accompanied by northward and southward magnetic fields, respectively [e.g., *Nishida et al.*, 1981; *Hayakawa et al.*, 1982]. These results indicate that fast flows originate from reconnection in a statistical sense. However, earthward flows are weaker evidence for reconnection than tailward flows, because the geomagnetic field is usually northward in the tail. It is also difficult to associate all earthward flows inside ~30 R_E with the formation of NENL, since earthward flows also originate from the DNL. Moreover, earthward fast flows inside ~30 R_E often originate from the tailward retreating NENL located tailward of the satellite in the substorm recovery phase, not at the time of substorm expansion onset [*Baumjohann et al.*, 1999; *Nakamura et al.*, 2001a; *Shue et al.*, 2003; *Ieda et al.*, 2004]. On the other hand, tailward flows inside ~30 R_E should originate from the NENL, not from the DNL. Tailward flows are also expected to be observed immediately following the formation of NENL, and are not expected to be observed after the retreat of the NENL to the tailward side of the satellite. Tailward flows are better associated with global auroral activity than are earthward flows [*Shue et al.*, 2003; *Ieda et al.*, 2003]. For these reasons, tailward flows were employed here to indicate the initiation of near-earth reconnection.

2. Data Set

2.1. Geotail Satellite and the Tsyganenko Model

[8] Geotail was launched on 24 July 1992 and was near the equatorial plane between 9 and 31 R_E during the interval from March 1996 through April 2001 that we surveyed to identify auroral breakup events. The apogee of Geotail was on the nightside in winter. The low-energy particle (LEP) instrument on board Geotail measures three-dimensional plasma distribution from 32 eV/q to 39 keV/q in one-spin period (~3 s) [*Mukai et al.*, 1994]. In this study, we used 12-s averages of ion velocity moments, calculated on the assumption that all ion species are protons. Corresponding 12-s averages of the magnetic field data obtained by the magnetic field (MGF) experiment [*Kokubun et al.*, 1994] were also used in statistical studies and 3-s averages are shown in case studies.

[9] The aberrated geocentric solar magnetospheric (AGSM) coordinate system was adopted with an angle of 4° for Geotail locations and data. For example, the aberration results in a typical satellite Y location shift of ~2 R_E toward the dawn with the satellite located 30 R_E down the tail. The Z locations shown in case studies are relative distance from a neutral sheet model [*Li and Xu*, 2000].

[10] Before reconnection occurs, each location in the magnetotail is connected to a location in the polar ionosphere by a geomagnetic field line. The foot point of Geotail locations on the ionosphere, assumed at 110 km above the ground, is calculated with a geomagnetic field line model. The Tsyaganenko 96 (T96) model [*Tsyganenko and Stern*, 1996] with the IGRF-10 model [*Macmillan and Maus*, 2005] was used. The T96 input parameters include the solar wind (the dynamic pressure, B_y, and B_z) from OMNI [*King and Papitashvili*, 2005] 1-min data, which were time-shifted to bow shock nose. The SYM-H index [*Iyemori*, 1990] was also used as a proxy of the ring current.

[11] These input parameters were 1-hour averages of the original 1-min values before breakups ($-60 \leq T < 0$ min). On the other hand, Geotail location in the tail at 2.5 min after breakup was used as input for T96. These selections mean that we have calculated the foot point before breakup for the Geotail location in the tail at breakup. The accuracy of the T96 model is not well known even before breakup. We thus used the calculated Geotail foot point as a reference in discussion of other results.

2.2. Polar Satellite Ultraviolet Images

[12] Polar was launched on 24 February 1996 and its 9 R_E apogee gradually shifted from the northern pole to the equator so that more breakups were observed in earlier years. The Polar ultraviolet imager (UVI) [*Torr et al.*, 1995] provides global imaging of auroras with a frame rate of 4 or 5 images per ~3 min. UVI images are taken in wavelength including the N_2 Lyman–Birge–Hopfield long (LBHL, ~1700 Å) and short (LBHS, ~1500 Å), and OI ~1304 Å and ~1356 Å. The spatial resolution of the images is ~40 km when Polar vertically observes the polar ionosphere from its apogee of 9 R_E. Images were projected to the assumed emission altitude of 120 km, and then were mapped to the modified APEX coordinates [*Richmond*, 1995] at 110 km from the ground.

[13] Original UVI images are smeared about 10 pixels in one CCD direction due to the satellite spin-associated wobbling [e.g., *Germany et al.*, 1998; *Frank et al.*, 2001]. This smearing typically corresponds to ±5° in longitude or ±2° in latitude on the auroral ionosphere when Polar is at the apogee. Because of the sinusoidal wobbling, a pair of

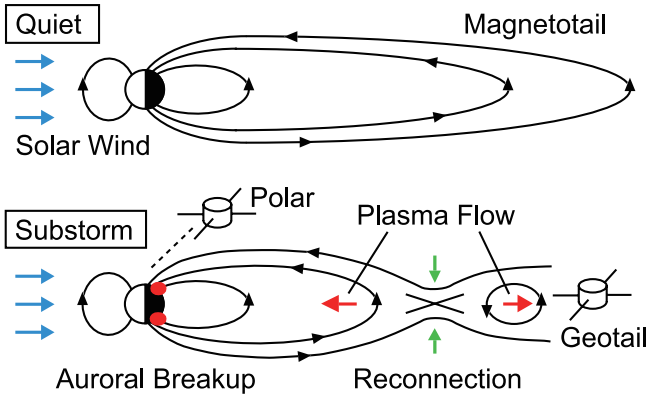

Figure 1. Schematic of magnetotail during quiet times and substorms. An auroral breakup in the polar ionosphere is remotely observed by the Polar satellite. Magnetic reconnection in the near-earth magnetotail is identified from in situ Geotail satellite observations of a tailward flow with southward magnetic field.

two pixels separated by 10 pixels are most sensitive to the aurora located at the midpoint of the two pixels. An auroral arc is thus often recorded as double arcs.

[14] Auroral images in case studies are corrected for the smearing, assuming that an aurora that actually exists at a target pixel is recorded by two pixels which are separated by ±5 pixels from the target pixel. This correction had not been confirmed to be successful for all events, so in statistical studies breakups were identified primarily with original images, taking manually the smearing into account. The smearing affects the identification of breakup location much less than ~5° in longitude even in original images, since the center of the smeared brightening represents the actual onset location.

3. Case Study

[15] Figure 1 illustrates an observation of auroral breakup and reconnection by satellites. The upper panel shows the quiet time magnetotail on the meridian plane, where the solar wind can be seen to stretch the earth's magnetic field. These stretched field lines are often thought to reconnect at the expansion onset of substorms as shown in the lower panel. Reconnection yields a pair of earthward and tailward flows. The tailward flows, used in this study to identify reconnection, exhibit helical field lines known as plasmoids, which are observed as north-then-south variations in the magnetic field as a plasmoid passes the satellite. Earthward flows are considered to be the cause of auroral breakups in the near-earth reconnection model of substorms [e.g., *Baker et al.*, 1996; *Shiokawa et al.*, 1998]. However, in other substorm models, reconnection is not regarded as the cause of auroral breakup [e.g., *Lui*, 1996].

[16] Figure 2 shows an auroral breakup beginning around 0725 UT on 12 January 1997. The upper panel shows a 20-min series of Polar satellite UVI images of the nightside polar ionosphere from 60 to 90° magnetic latitude in the modified APEX coordinates. One LBHL image is shown among four images taken every 3 min. The images reveal a brightening in the center panel (0725:12 UT), involving a rapid poleward expansion as can be seen in the later panels. This expansion is considered to be an essential characteristic of auroral breakup.

[17] The lower panel shows simultaneous Geotail satellite observations of the north–south component of the magnetic field (B_z) and the sunward–tailward component of the plasma velocity (V_x) measured near the equatorial plane in the magnetotail at a distance of 29 R_E down the tail. A north-then-south variation in B_z was observed, associated with tailward plasma flows in V_x, indicating the passage of a looped or helical magnetic field structure (i.e., a plasmoid). The center of the plasmoid illustrated in Figure 1 corresponds to the north-to-south transition in B_z at 0724:47 UT, simultaneous with breakup.

[18] The northward-oriented magnetic field in the leading half of the plasmoid represents additional evidence that the tailward flow is caused by reconnection. While plasmoids are more convincing evidence of reconnection than tailward flows, it is more difficult to automatically identify plasmoids than tailward flows. Tailward flows were thus employed exclusively in this study to identify near-earth reconnection, implicitly assuming that the identified tailward flows are associated with plasmoids and reconnection.

[19] The white circles in the UVI images in Figure 2 indicate the Geotail foot point on the ionosphere, calculated using T96 with the dynamic pressure = 3.9 (nPa), B_y = 4.8 (nT), and B_z = −2.0 (nT) in the solar wind and with SYM-H = −15.3 (nT). The foot point location (23.0 MLT) is near the auroral breakup location (22.8 MLT). The close temporal and spatial association between breakup and

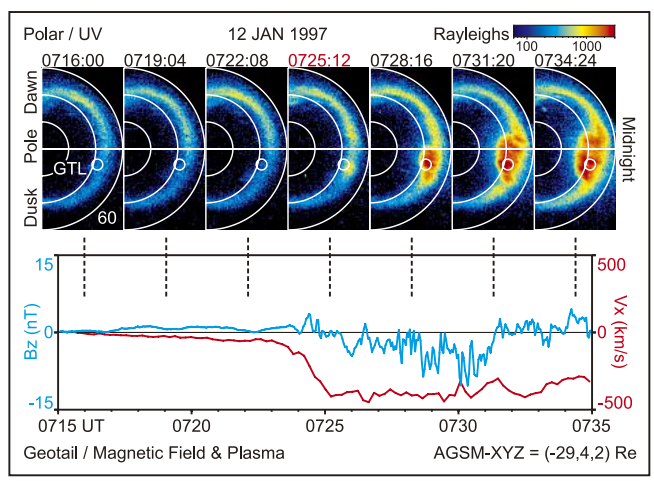

Figure 2. Time series showing a reconnection-related plasmoid/tailward flow observed near the time and longitude of an auroral breakup. The upper panels show Polar ultraviolet images of the nightside polar ionosphere in the modified APEX coordinates at 110 km altitude. Auroral emissions in Lyman–Birge–Hopfield long (1700 Å) are shown in false color. The breakup at 22.8 magnetic local time (MLT), 66.3° latitude is seen in the 0725:12 UT image. White circles in the images indicate the Geotail location mapped into the ionosphere at 23.0 MLT, 68.6° latitude. The lower panel shows Geotail magnetic field and plasma observations of the magnetotail in the AGSM coordinates. A tailward flow with north-then-south variation at 0724:47 UT in the magnetic field indicates the passage of plasmoid.

plasmoid/tailward flow suggests that the magnetic reconnection process is intimately related to the auroral breakup.

4. Statistical Study

4.1. Identification of Auroral Breakup

[20] Auroral breakups (substorms) are often discriminated from localized brightenings including pseudo-breakups and auroral poleward boundary intensifications (PBIs). Pseudo-breakups apparently result from essentially the same physical process as auroral breakups, but do not lead to full breakup for unknown reasons [*Pulkkinen et al.*, 1998; *Rostoker*, 1998; *Fillingim et al.*, 2000]. PBIs are often accompanied with earthward flows and are related to the activation of the DNL [*de la Beaujardière et al.*, 1994; *Lyons et al.*, 2002]. In this study, breakups were distinguished from pseudo-breakups and PBIs by the observation of poleward expansion, which is a major characteristic in the original definition of substorms as proposed by *Akasofu* [1964].

[21] Auroral breakups are often preceded by pseudo-breakups. It is thus often less clear whether flows prior to breakups are associated with the breakup or the preceded pseudo-breakup. For this reason, isolated breakups are best compared with simultaneous flow observations. However, definitely isolated breakups are quite rarely observed in global images. We thus selected relatively isolated breakups that may include very weak/localized preceding brightenings.

[22] The list of breakup events was constructed as follows. (1) Breakups were first identified visually as auroral brightening followed by poleward expansions greater than $\sim 2°$ in 10 min. Breakups occurring within 20 min of a previous breakup were then excluded. Breakup events were also excluded if there were precursor brightenings within 10 min before breakups ($-10 \leq T < 0$) with their poleward expansion more than $\sim 1°$ in visual inspection.

[23] (2) The onset times were chosen as the center time between images before and after brightening. The times of images were chosen as the center of the image accumulation period (18.4 or 36.8 s). The time resolution of UVI images are typically between 28 and 83 s. In reality, however, it was often subjective to determine the onset time in the time resolution less than ~ 1 min, because very sudden breakups are rare on this timescale. We used breakups only when the identified onset times appeared to include uncertainty of less than 3 min (±1.5 min), as the UVI usually takes at least one LBHL image every 3 min. Breakups were identified primarily using LBHL images, which represent precipitating electron energy flux. Other wavelength images were also referred to if available in order to determine the detailed onset timings and location of the breakup.

[24] (3) We set a lower limit in the breakup strength, which is an increase in the auroral power more than 2 GW. The increase was calculated comparing the maximum auroral power in $-10 \leq T < 0$ and in $0 \leq T < 10$ min. The auroral power was calculated by integrating the precipitating electron energy flux over 60–80° in latitudes and ±1 hour MLT from breakup MLTs. The energy flux was estimated from LBHL images [e.g., *Lummerzheim et al.*, 1997; *Germany et al.*, 1997]. We assumed that the energy flux was related to the LBHL surface brightness by 130 Rayleighs per mW m^{-2} s^{-1}, referring to the results by *Germany et al.* [2001] and *Galand and Lummerzheim* [2004]. The surface brightness is related to the photon flux to the instrument aperture by 30 Rayleighs per photons cm^{-2} s^{-1}.

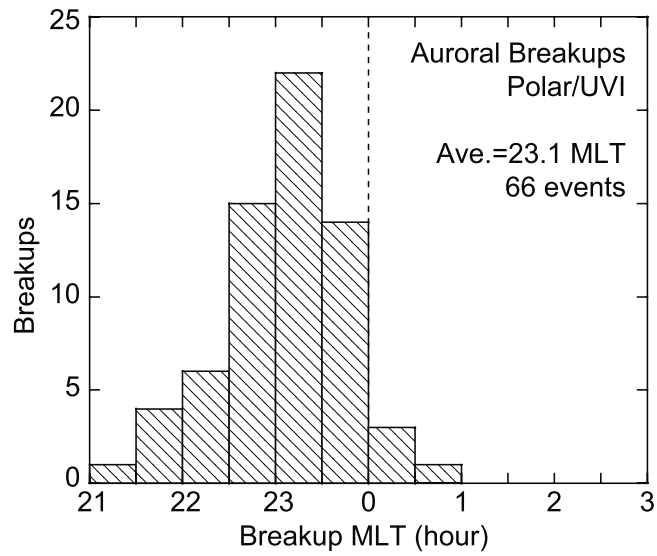

Figure 3. Magnetic local time (MLT) distribution of isolated auroral breakups identified from Polar ultraviolet imager images. The average and the median are both 23.1 MLT. Geotail was required to be located at $-25 > X_{AGSM} \geq -31\ R_E$ and $|Y_{AGSM}| < 15\ R_E$ 2.5 min after breakup. Geotail was also required to be in the central plasma sheet in the interval 5–10 min before breakup.

[25] (4) Geotail was required to be in the central plasma sheet of the magnetotail in the interval 5–10 min prior to a given breakup in order to maximize the probability that Geotail would measure any breakup-related flow. The definition of the central plasma sheet is given below. Geotail was also required to be in the magnetotail beyond 25 R_E and within its 31 R_E apogee down the tail and inside 15 R_E dawn–dusk distance from the tail axis at 2.5 min after a given breakup without significant data gaps in the magnetic field and plasma observations. As plasmoids are more often observed beyond $\sim 25\ R_E$ than within this distance [*Ieda et al.*, 1998], tailward flows were also studied in the region beyond 25 R_E in this paper.

[26] Figure 3 shows the MLT distribution of the 66 breakups identified from 5 December 1996 through 9 February 2001 using this procedure. We visually determined a breakup MLT as the center of a brightening. The breakup longitude is clustered in the premidnight region, and the average and median breakup longitudes are both 23.1 MLT. This is consistent with the known fact that breakups usually occur in the premidnight region [e.g., *Liou et al.*, 2001].

[27] In our preliminary study we first newly identified all breakups (about 500 events) for Geotail in the tail beyond 25 R_E. However, the preliminary study was not very successful because the association between flows and breakup was less clear for breakups that were not isolated. We thus concentrated on isolated breakups and this reduced the number of breakups.

4.2. Definition of Magnetotail Region and Tailward Flow

[28] The time window defined for each breakup event extends from 20 min before the event through 40 min after

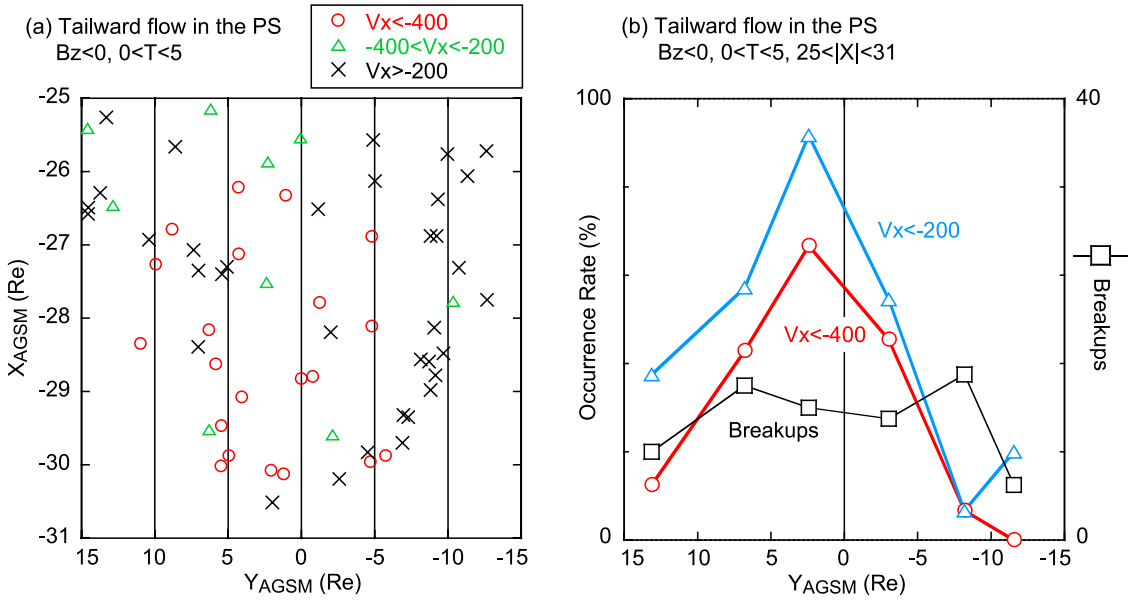

Figure 4. Geotail observations of tailward flows with southward magnetic field in the plasma sheet 0–5 min after 65 auroral breakups. (a) Occurrence and magnitude of tailward flow with respect to Geotail location on the equatorial (*XY*) plane of the tail. (b) Occurrence rate of tailward flow with respect to Geotail *Y* location.

breakup initiation, subdivided into 5-min intervals. The position of Geotail in the magnetotail region in each 5-min interval was then determined as follows.

[29] (1) All Geotail data in this study were assumed to be obtained either in the plasma sheet (PS) or in the tail lobe (Lobe), where the PS consists of a central plasma sheet (CPS) and a plasma sheet boundary layer (PSBL).

[30] (2) The plasma beta was calculated for each 12-s ion and magnetic field data point under the assumption that the ratio of ion to electron temperature is 5 [*Slavin et al.*, 1985]. Each 12-s data point was then classified as CPS ($\beta \geq 1$), PSBL ($0.1 \leq \beta < 1$), or Lobe ($\beta < 0.1$).

[31] (3) A 5-min interval was labeled CPS, if the ratio of the number of CPS samples to the total (CPS, PSBL, and Lobe) number of samples was more than 50%. Lobe intervals were determined in the same way. Intervals not satisfying either of these conditions were labeled PSBL intervals. CPS and PSBL intervals were regarded as PS intervals ($\beta \geq 0.1$). Note that a breakup event can include both PS intervals and Lobe intervals, but only PS intervals will be studied.

[32] "Tailward flow" refers to "tailward flow with southward magnetic field" in this statistical study. Tailward flows were identified in PS as follows. For each 5 min PS interval, the maximum tailward velocity ($-V_x$) among the 12-s PS samples with southward magnetic field ($B_z < 0$) was determined. (Lobe samples in the PS interval were not used.) If the maximum tailward velocity was equal to or greater than 200 km/s ($V_x \leq -200$ km/s), a tailward flow was considered to have been observed in the relevant 5-min PS interval. Tailward flows with velocity in the range $-400 < V_x \leq -200$ km/s were classified as moderate, and flows with velocity in the range $V_x \leq -400$ km/s were categorized as fast. The occurrence rate of tailward flow events was calculated for each 5-min interval as the ratio of the number of tailward flow events to the total number of breakups with Geotail in PS.

4.3. Dawn–Dusk Locations of Tailward Flow

[33] Figure 4 shows Geotail observations of tailward flows between 0 and 5 min after auroral breakups ($0 \leq T < 5$ min) in $-25 > X_{AGSM} \geq -31$ R_E and $|Y_{AGSM}| < 15$ R_E. Geotail was in the plasma sheet at this time for 65 of 66 breakups in our list. This high occurrence of the PS event is due to the selection criteria of breakup mentioned before, which require that Geotail has stayed in the CPS 5–10 min prior to breakup. The remaining 1 event is not shown because Geotail was in the tail lobe at this time.

[34] Figure 4a shows Geotail *XY* locations on the equatorial plane for 65 breakup events. Each symbol represents a Geotail location for each breakup. Red circles indicate that Geotail observed relatively fast tailward flows ($V_x \leq -400$ km/s). Green triangles indicate that Geotail observed moderate tailward flows ($-400 < V_x \leq -200$ km/s). Black crosses indicate that Geotail observed no ($V_x > -200$ km/s) tailward flows. Most tailward flows (red circles and green triangles) were observed in $-5 \leq Y < 10$ R_E, outside of which tailward flows were rare.

[35] Figure 4b shows the occurrence rates of tailward flows against *Y* in each 5 R_E bin. The red line with circles indicates the occurrence rates of the fast tailward flow ($V_x \leq -400$ km/s) events, which is the ratio of the number of red circles to all symbols shown in Figure 4a. The blue line with triangles shows the occurrence rates of all tailward flow ($V_x \leq -200$ km/s) events, which is the summation of fast tailward flows and moderate tailward flows. The black line with squares shows the number of breakup events against *Y*. It was confirmed that tailward flows tended to be observed in $-5 \leq Y < 10$ R_E, where the occurrence rate of all tailward flows was 68%, and fast tailward flows

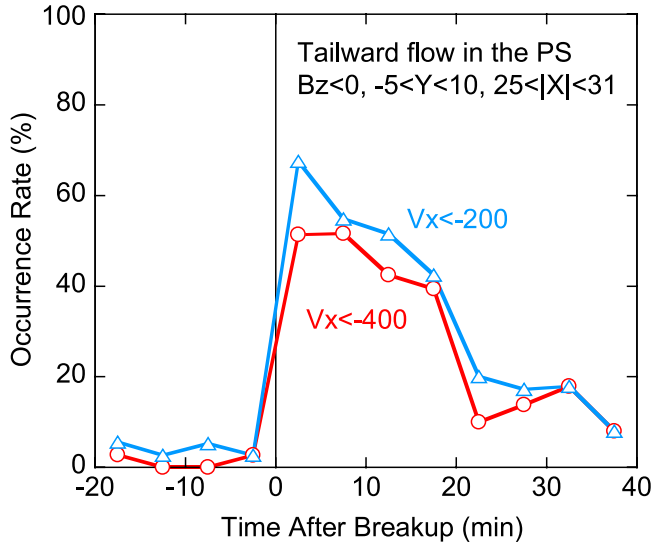

Figure 5. Temporal variations in the occurrence rate of tailward flow with southward magnetic field for auroral breakups when Geotail was in the plasma sheet at $-25 > X_{AGSM} \geq -31$ R_E and $-5 \leq Y_{AGSM} < 10$ R_E. The occurrence rate is computed for each 5-min interval as the ratio of the number of tailward flow events to the number of breakups with Geotail in the plasma sheet. The number of breakups is 38 at $-10 \leq T < -5$ min and varies with time.

occurred in 51% of the 37 cases of breakup. The occurrence rates appear highest between $0 \leq Y < 5$ R_E, where tailward flows occurred in 92% of cases, and fast tailward flows were observed in 67% of the 12 cases. This peak location is consistent with the preferred location ($Y_{AGSM} \sim 3$ R_E) of plasmoids [*Ieda et al.*, 1998].

4.4. Temporal Evolution of Tailward Flow

[36] Figure 5 shows the temporal evolution of tailward flows observed in $-5 \leq Y < 10$ R_E. The red line with circles indicates fast tailward flows ($V_x \leq -400$ km/s), and the blue line with triangles indicates all (fast and moderate) tailward flows ($V_x \leq -200$ km/s), as in Figure 4b. There is a sharp increase in the occurrence rates of fast and all tailward flows at breakups ($T = 0$). This development of the tailward flows implies that reconnection was often initiated in the magnetotail at the time of breakup.

[37] The two lines (fast and all tailward flows) were qualitatively similar, indicating that there is no qualitative difference between fast and moderate tailward flows in association with breakup, and presumably also with reconnection. In this regard, the occurrence rate of reconnection would be underestimated if we employed $V_x \leq -400$ km/s as criteria of tailward flows. The criterion of $V_x \leq -200$ km/s was thus considered to better represent the occurrence rate of reconnection.

[38] Tailward flows were rarely observed before breakups, despite the expectation that tailward flows associated with precursor brightening would be observed [*Ieda et al.*, 2001]. Tailward flows were rare before breakup, presumably because the present data set only includes breakups without significant precursor brightening. The rareness of tailward flows before breakup may also indicate that such precursor-associated flows are more localized than breakup-associated flows.

[39] After breakup, the occurrence rate of tailward flows gradually decreased with time. Plasmoids are typically observed in the leading edge of tailward flows and have a timescale of 1 min [*Ieda et al.*, 1998, 2001]. Thus these late tailward flows are thought to be postplasmoid flow as also seen in Figure 2, or associated with multiple breakups. There is a weak indication of a rapid decrease in the occurrence rate at 20 min after breakup. This suggests that postplasmoid flows typically continue ~20 min inside ~30 R_E down the tail.

4.5. Longitudinal Association

[40] Figure 6 shows the association between the magnetic local time (MLT) of breakups and the Y location of tailward flows. Figures 6a and 6b are shown in the AGSM and GSM coordinates, respectively. The tailward flows shown were observed in the first 5 min ($0 \leq T < 5$ min) of breakups, corresponding to the interval in which the occurrence rate of tailward flows increased sharply (see Figure 5). Each symbol indicates the same as in Figure 4a.

[41] Tailward flows tended to appear on the dusk side when breakups occurred on the dusk side, and near midnight for midnight breakups in Figure 6a. This result implies a longitudinal association between tailward flows and breakups. A least squares fitting for fast tailward flows ($V_x \leq -400$ km/s) gives a regression line of

$$Y_{AGSM} = -5.72 \times (MLT_{BUP} + 0.635) \quad (1)$$

with a correlation coefficient (R) of 0.80. Note that this regression line was obtained using the relative MLT (e.g., 23 MLT corresponds to −1 MLT). The regression line for all tailward flows ($V_x \leq -200$ km/s) was $Y_{AGSM} = -6.08 \times$ (MLT + 0.567), $R = 0.67$ (not shown). The lower coefficient for all tailward flows may be due to the inclusion of slower flank portions of tailward flow under the relatively relaxed criterion of $V_x \leq -200$ km/s. It is thus assumed that the regression line for $V_x \leq -400$ km/s better represents the longitudinal relationship between breakups and the center of tailward flows.

[42] As shown in Figure 6b, the regression line in the GSM coordinates instead was

$$Y_{GSM} = -5.70 \times (MLT_{BUP} + 0.288) \quad (2)$$

with $R = 0.80$. This line was shifted ~2 R_E duskward, when compared to the equation (1). Except for the typical shift of 2 R_E, Figures 6a and 6b appear similar with the particular data set used in this study.

5. Discussion

5.1. Field Line Mapping

[43] We have obtained the relationship between the Y location of tailward flow/reconnection and breakup MLT in the equations (1) and (2). To clarify the implication of this relationship we calculated the foot point of Geotail locations on the ionosphere, assumed at 110 km above the ground.

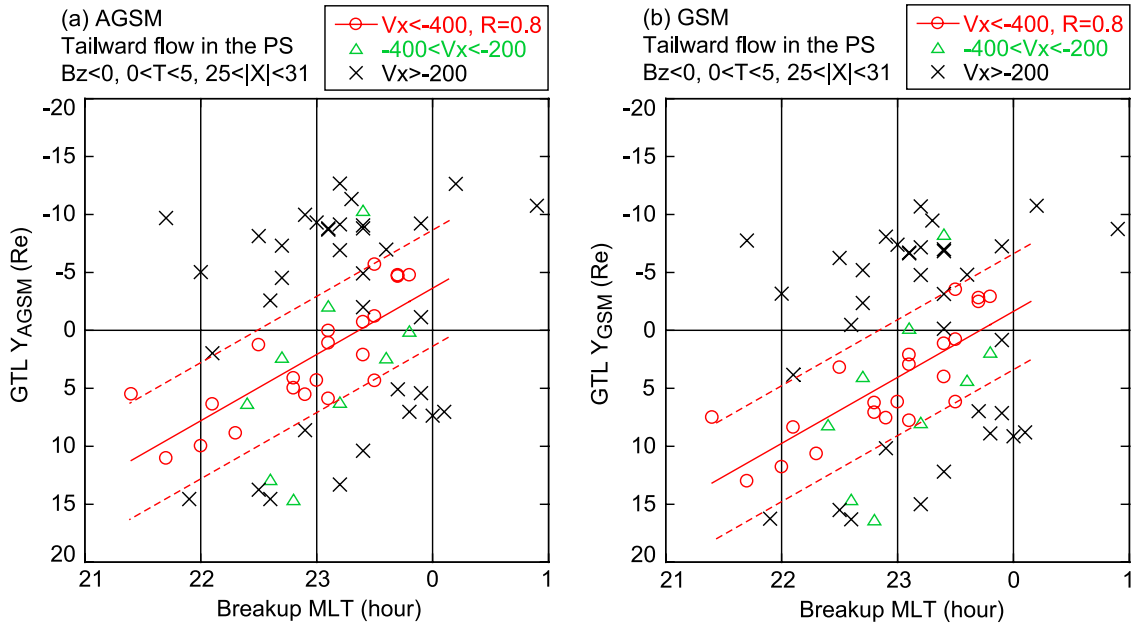

Figure 6. Longitudinal relationship between breakup and tailward flow in the first 5 min following 65 breakup onsets shown in (a) AGSM and (b) GSM coordinates. The red solid lines represent the regression lines for fast tailward flows ($V_x \leq -400$ km/s), which are $Y_{AGSM} = -5.7 \times (\mathrm{MLT} + 0.6)\ R_E$ for Figure 6a and $Y_{GSM} = -5.7 \times (\mathrm{MLT} + 0.3)\ R_E$ for Figure 6b. Dashed lines 5 R_E from the regression lines are shown for reference.

[44] As a result, the Geotail Y locations were related to the MLT of the Geotail foot points for fast tailward flows (not shown) by

$$Y_{AGSM} = -5.16 \times (MLT_{FP} + 0.313) \quad (3)$$

where R = 0.93. The average X_{AGSM} location was $-28\ R_E$. The inclination of -5.72 in the equation (1) is slightly steeper than the mapping factor of -5.16 in the equation (3) just obtained. This result might indicate that breakup tends to occur somewhat closer to ~23 MLT even when reconnection occurs away from ~23 MLT. The second term (0.313) of the equation (3) is presumably due to the aberration, because the tail axis maps to ~23.7 MLT on average. Thus the second term (0.653) of the equation (1) consists of 0.3 by the aberration and another 0.3, which suggests a dawnward displacement of tailward flows from breakup MLT.

[45] Figure 7 shows the relationship between breakup MLT and MLT of the Geotail foot point. Each symbol indicates the same as in Figure 4a. MLT of the Geotail foot point was related to breakup MLT as

$$MLT_{FP} = 1.07 \times (MLT_{BUP} + 0.329) \quad (4)$$

with R = 0.83 for fast tailward flows ($V_x \leq -400$ km/s). Three dashed lines represent $dMLT \equiv MLT_{FP} - MLT_{BUP}$ = 1, 0, -1 hour for references. The inclination of 1.07 is slightly steeper than unity. This results might also indicate the preference of breakups to occur near ~23 MLT. However, it is probably more reasonable to interpret that the inclination is unity. Tailward flows typically occurred inside dMLT = ±1 hour, with a weak indication that tailward flows were observed somewhat dawnward from the breakup MLTs. dMLT was 0.29 (corresponds to ~2 R_E) at MLT_{BUP} = 23.1, which is the average breakup MLT in Figure 3. However, this 0.3-hour dawnward displacement is not statistically significant because the standard deviation was 0.5 hour and there were few events near $dMLT = -0.5$ hour in Figure 7.

[46] In summary, we infer that tailward flow occurs near breakup MLT. This interpretation corresponds to modifications of the equations (1) and (2) as

$$Y_{AGSM} = -5.2 \times (MLT_{BUP} + 0.3) \quad (5)$$

$$Y_{GSM} = -5.2 \times MLT_{BUP} \quad (6)$$

[47] The 0.3-hour dawnward displacement of tailward flows from breakup MLT may be consistent with the 0.4-hour dawnward displacement of earthward flows from pseudo-breakups found by *Nakamura et al.* [2001b]. They interpreted that this displacement was consistent with the idea that the aurora corresponds to an upward field-aligned current at the dusk side of the flows. Thus flows are expected to be shifted dawnward from breakup, too. However, this expectation is not readily granted, because breakup-associated earthward and tailward flows were observed in the postmidnight and premidnight, respectively, in Figure 3f in the study by *Nagai et al.* [1998].

5.2. Width of Tailward Flow and NENL

[48] If the tailward flows occur over a wide lateral area across the tail, no longitudinal association between breakups and tailward flows should be found. Thus the longitudinal association also indicates that tailward flows are longitudinally localized. As shown in Figure 6, most tailward flows

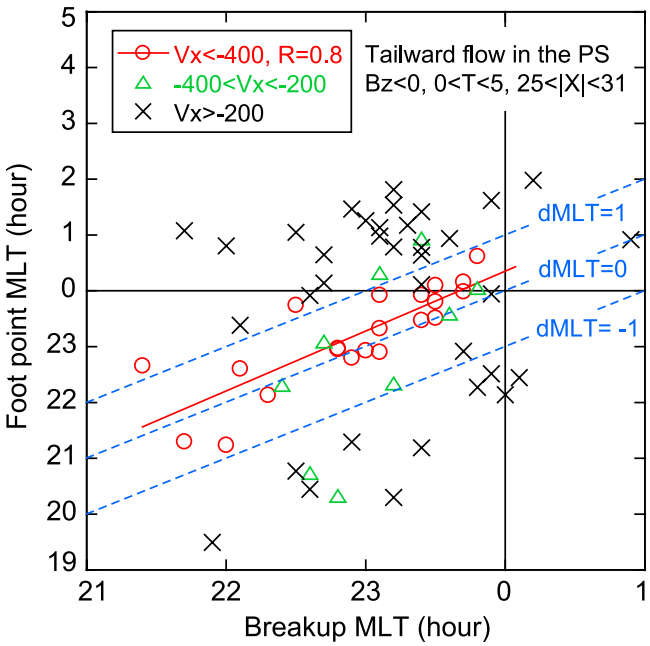

Figure 7. Magnetic local time (MLT) location of breakup and Geotail foot point in the first 5 min following 65 breakup onsets. The red solid line represents the regression line of $MLT_{FP} = 1.07 \times (MLT_{BUP} + 0.3)$, with a correlation coefficient of 0.8 for fast tailward flows ($V_x \leq -400$ km/s). Dashed lines are shown for reference.

were observed inside the dashed lines, which represent ±5 R_E from the regression lines. Outside the dashed lines, tailward flows were rarely observed. It is thus inferred that the typical Y width of tailward flows is of the order of 10 R_E, or 2 hours in MLT as seen in Figure 7.

[49] This width is wider than the width of earthward flows previously inferred as less than ~6 R_E [*Angelopoulos et al.*, 1997; *Nakamura et al.*, 2001b]. This difference is presumably due to the expansion of plasmoids [*Ieda et al.*, 1998]. Accordingly, the width of the NENL is expected to be narrower than 10 R_E. Breakup-associated flow had been less frequently observed in the near tail than in the distant tail as mentioned in the Introduction. This is presumably because flows are localized around breakup MLT in the near tail. Tailward flow appears better indicator of the initiation of near-earth reconnection than earthward flow, because it is wider, as well as because of the reasons in the Introduction.

5.3. Tailward Flow Near Breakup MLT

[50] Figure 8 shows the temporal variation of the occurrence rate of tailward flows in the same format as in Figure 5, except that the occurrence rate was calculated inside the dashed lines in Figure 6a, which represent ±5 R_E from the regression line, for breakups between 22 and 0 MLT. The variation in Figure 8 is qualitatively similar to that in Figure 5, where $-5 \leq Y < 10$ R_E was considered, but tailward flows occurred more often (88% of the 26 cases) in Figure 8 in the first 5-min interval ($0 \leq T < 5$ min) following breakup. This higher occurrence rate confirms that breakups are accompanied by tailward flows near breakup MLT at least in most cases. The NENL is inferred to usually be formed inside 25 R_E down the tail, because tailward flows were almost always observed beyond 25 R_E.

[51] Tailward flows were not observed for only two breakups when Geotail was well inside 5 R_E from the predicted Y locations in Figure 6. These two events were an earthward flow event and a traveling compression region event, as will be shown later. We thus consider that the two events are not inconsistent with the initiation of the near-earth reconnection. Auroral breakup is thus likely to always be associated with near-earth reconnection near breakup MLT.

[52] On the other hand, the reverse is not in the case. Tailward flows are not always associated with breakup [*Ieda et al.*, 2001], while tailward flows inside 30 R_E are almost always associated with auroral brightening, which may be weak or spatially limited. Reconnection is therefore considered to insufficient as a condition for auroral-breakup (substorm).

5.4. Breakups Without Tailward Flow

5.4.1. An Earthward Flow Event

[53] Figure 9 shows one of the two breakups without tailward flows even near the expected Y location of tailward flows as found in Figure 6. The breakup initiated at 2321:39 UT on 3 February 1997 and was accompanied by an earthward flow. Figure 9a is a 24-min series of Polar UVI images of the nightside polar ionosphere. The Polar images show a breakup in the panel of 2321:53 UT as labeled with red letters on the top of the image. This is the center time of the interval over which the image was taken. We define the onset time of the breakup (2321:39 UT) as the

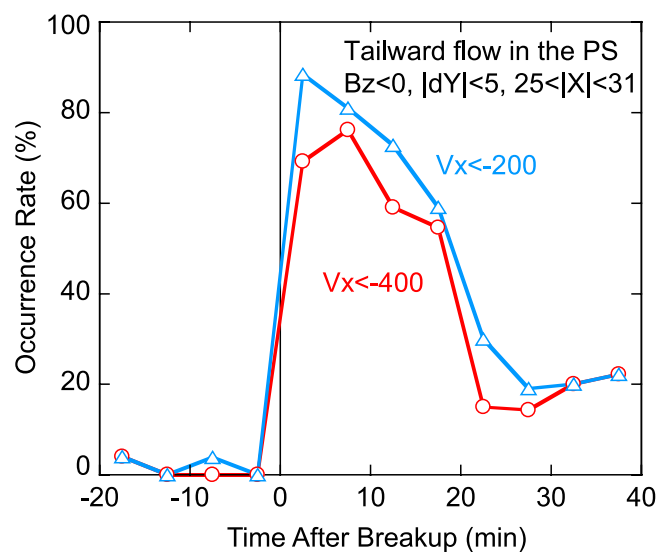

Figure 8. Temporal variations in the occurrence rate of tailward flow with southward magnetic field for auroral breakups between 22 and 0 magnetic local time (MLT) when Geotail was in the plasma sheet at $-25 > X_{AGSM} \geq -31$ R_E. Geotail was also required to be located within 5 R_E of the expected Y location of tailward flow as a function of breakup MLT, which is $Y_{AGSM} = -5.7 \times (\text{MLT} + 0.6)$ R_E. The occurrence rate is computed for each 5-min interval as the ratio of the number of tailward flow events to the number of breakups with Geotail in the plasma sheet. The number of breakups is 26 at $-10 \leq T < -5$ min and varies with time.

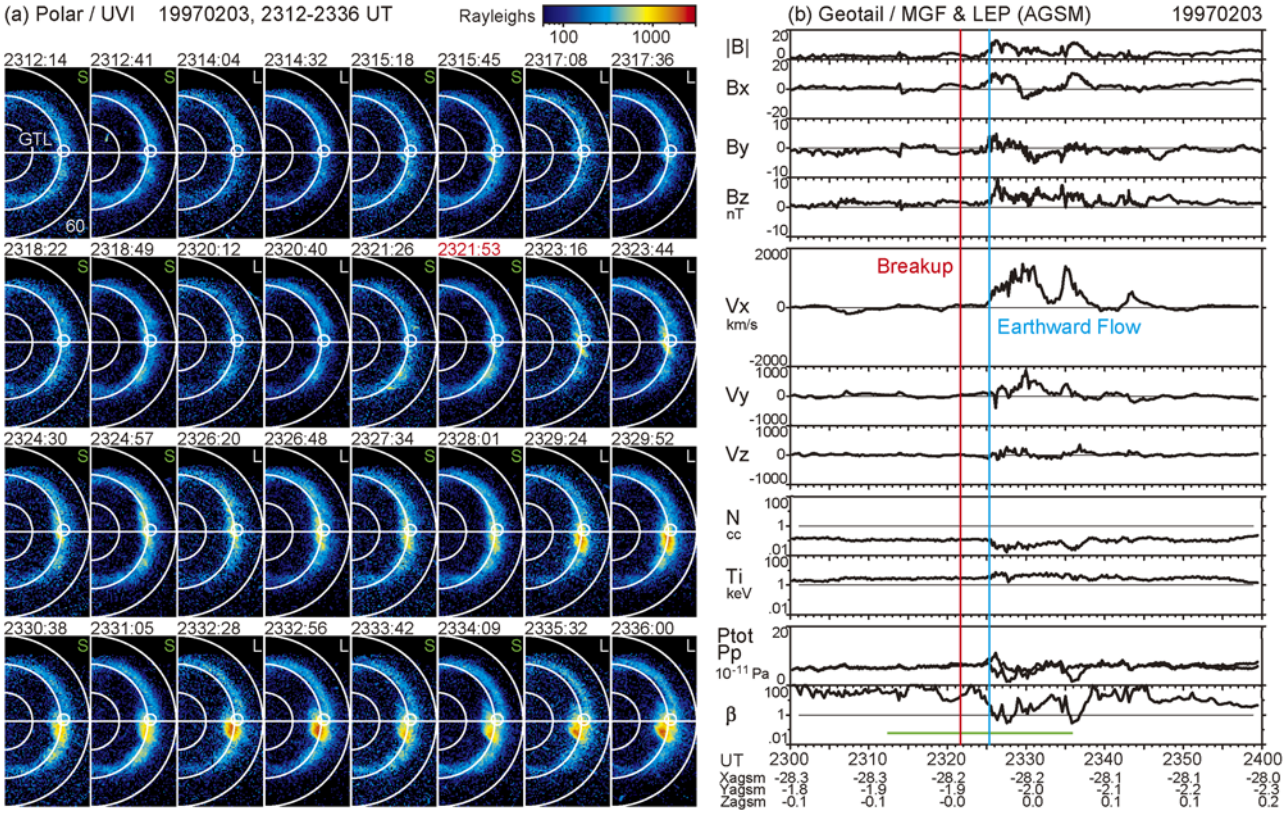

Figure 9. One of the two breakups without tailward flows. (a) Polar ultraviolet imager (UVI) observations of the nightside ionosphere. Full-time resolution images are shown with a sequence of two Lyman–Birge–Hopfield long images and two LBHS images. The breakup (23.4 MLT, 69.9° latitude) is first seen in the 2321:53 panel, which is labeled with red letters. White circles indicate the Geotail foot point (0.1 MLT, 69.1° latitude). (b) Geotail observation of the magnetotail. A green horizontal line shown in the bottom panel indicates the interval of Polar UVI images shown on the left. A red vertical line is the time of auroral breakup as identified by the UVI observations. A blue vertical line marks the initiation of an earthward flow faster than 200 km/s. The first four panels show the 3-s magnetic field data. The next five panels are 12-s ion velocities, density, and temperature. In the next panel the static total pressure (thermal pressure plus magnetic pressure) and the thermal pressure are superposed, where the ratio of ion to electron temperature is assumed to be five. The bottom panel is the plasma beta (ratio of the thermal pressure to the magnetic pressure).

center time between the time the brightening was first identified (2321:53 UT) and the time of the previous image (2321:26 UT).

[54] The white circles in UVI images indicate the Geotail foot point on the ionosphere at 2.5 min after breakup, calculated using T96 with the dynamic pressure = 1.1 (nPa), $B_y = -1.0$ (nT), and $B_z = -2.2$ (nT) in the solar wind and with SYM-H = −8.8 (nT). The foot point location (0.1 MLT) is somewhat (0.7 hours) dawnward of breakup at 23.4 MLT.

[55] Figure 9b shows corresponding Geotail observation at AGSM $(X, Y, Z) = (-28, -2, 0)\ R_E$. A green line on the bottom panel is the interval of UVI images shown in Figure 9a. A red vertical line marks the breakup at 2321:39 UT as identified in Figure 9a. A blue vertical line at 2325:20 UT indicates the initiation of an earthward flow determined by the first data sample with earthward velocity faster than 200 km/s. From top to bottom, 1 hour of the Geotail 3-s magnetic field and 12-s ion observations are shown. Detailed explanations are in the figure caption.

[56] The earthward flow was delayed from the breakup by 3.7 min. It is thus impossible to interpret that this particular earthward flow marks the initiation of the near-earth reconnection that causes auroral breakup. However, the fast earthward flow (694 km/s) is likely to be somehow associated with the reconnection process. The aurora appears to have shifted dawnward from 23.4 MLT in the 2321:53 UT panel (breakup) to 23.9 MLT in the 2326:48 UT panel (1.5 min after earthward flow). One possible interpretation of this event is thus that reconnection/flows first initiated somewhat duskward (23.4 MLT) of the Geotail location (0.1 MLT) and were not observed, and then the neutral line shifted dawnward closer to the Geotail longitude so that the earthward flow was observed later.

5.4.2. A TCR Event

[57] Figure 10 shows the other breakup without tailward flows in the same format as Figure 9. The breakup started at 0459:11 UT on 16 December 1996 and was accompanied by a TCR signature. Figure 10a shows Polar UVI observation of a breakup identified at 0459:11 UT between the 0458:57 and the 0459:25 UT panels. There is an intensification of

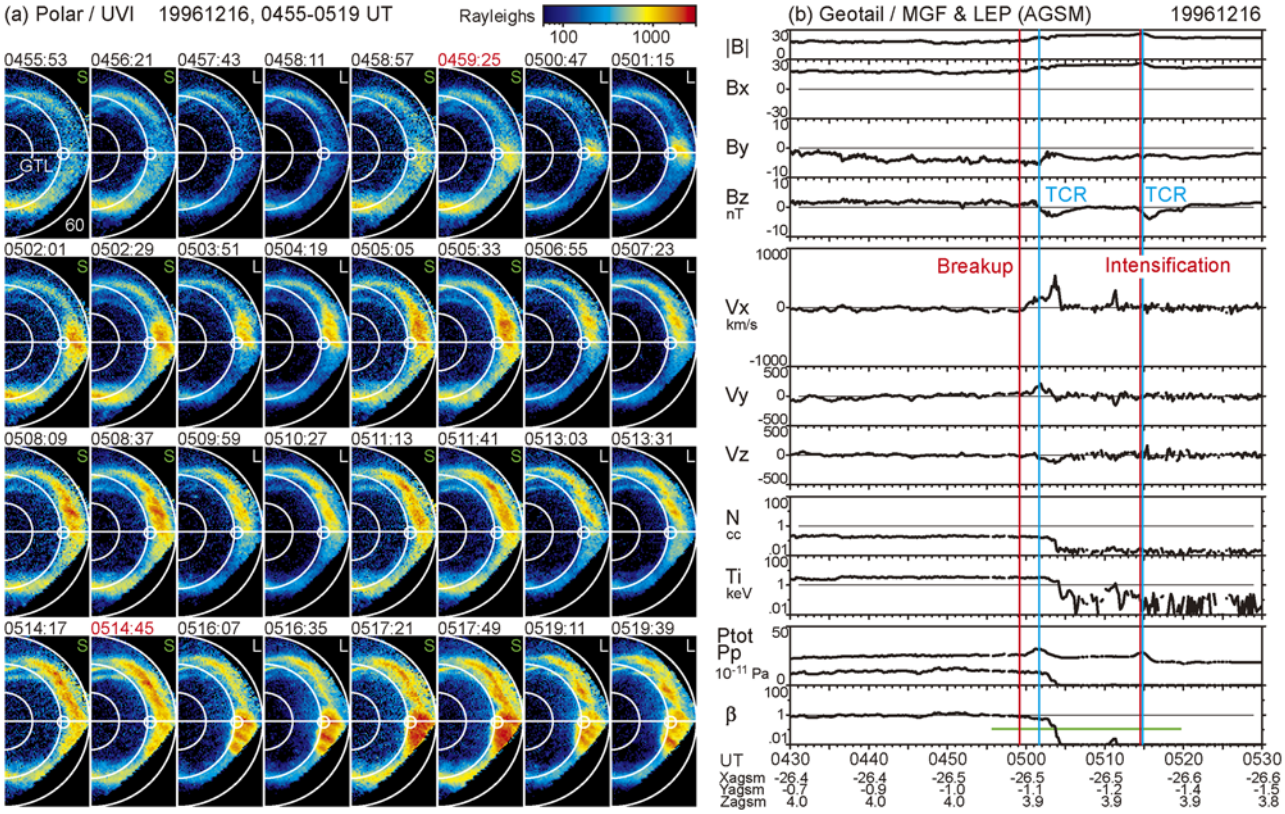

Figure 10. The other breakup event without tailward flows in the same format as Figure 7. (a) Polar ultraviolet imager images show an auroral breakup (23.9 MLT, 64.9° latitude) in the panel labeled as 0459:25 UT, and this breakup was estimated to have occurred at 0459:11 UT. An intensification of the breakup is seen in the 0514:45 panel and was estimated to have occurred at 0514:31 UT. White circles indicate the Geotail foot point (23.9 MLT, 69.2° latitude). (b) Geotail magnetic field and thermal ion parameters are shown. TCR signatures are observed with peaks in the total pressure at 0501:41 UT and at 0514:48 UT as marked with blue vertical lines.

the breakup at 0514:31 UT, which is the center of the 0514:17 UT and the 0514:45 UT panels. The white circles in UVI images in Figure 2 indicate the Geotail foot point, where the dynamic pressure = 3.2 (nPa), $B_y = -1.5$ (nT), and $B_z = -1.8$ (nT) in the solar wind and with SYM-H = -8.1 (nT). The foot point location (23.9 MLT) is the same as the auroral breakup location.

[58] Figure 10b shows corresponding Geotail observations in the magnetotail at $(X, Y, Z) = (-27, -1, 4)\ R_E$. A north-then-south variation in the magnetic field and an enhancement in the total pressure peaked at 0501:41 UT appears to indicate a passage of the center of a tailward-moving plasmoid 2.5 min after the breakup. However, a slow earthward flow was observed instead by Geotail in the PSBL ($0.1 \leq \beta < 1$). One possible interpretation for this discrepancy is that there was a tailward flow/plasmoid in the central plasma sheet, which was not directly observed but was remotely observed as a traveling compression region (TCR). A TCR typically has a north-then-south variation in the magnetic field and an enhancement in the magnetic strength, indicating tail lobe manifestation of a passage of a plasmoid released by near-earth reconnection [e.g., *Slavin et al.*, 1993]. In this particular event, such a plasmoid may have not yet fully developed to involve magnetic field lines in the PSBL. A similar TCR was reported by *Owen and Slavin* [1992], where they also found that about half of TCRs studied by *Slavin et al.* [1993] were in PSBL with energetic ion enhancements.

[59] Another TCR was observed at 0514:48, which lacked the northward variation in the magnetic field. This characteristic is considered as a remote indication of the formation of a NENL [*Taguchi et al.*, 1998]. This TCR is almost simultaneous with the intensification of the breakup at 0514:31 UT, suggesting a close temporal relationship in variations between auroras and the magnetotail for this particular event.

5.5. Timing of Reconnection and Auroral Breakup

[60] In this study we found that breakup was likely to always be accompanied by near-earth reconnection. To further clarify their cause-and-effect relationship, their relative timing is crucial. After inspection of all individual events, however, we found no convincing events where tailward flows were observed before breakups in our data sets based on Geotail and Polar observations. Tailward flows were rather detected in the first 5-min interval ($0 \leq T < 5$ min) following breakup initiation. However, this result does not necessarily indicate that reconnection was initiated after breakup, because the time delay between reconnection onset and the arrival of tailward flows at the satellite location should be considered. Assuming that this time delay is a few (2–3) min, breakup and reconnection are

inferred to initiate simultaneously with a temporal resolution of a few minutes.

[61] No definitive tailward flow event was observed to occur before breakup in this study. No irrefutably definitive event appears to have been reported in previous studies with a reconnection signature occurring before breakup in global images. The earliest plasmoids reported by *Ieda et al.* [2001] in a study of plasmoid-associated auroral brightening were observed ~2 min before a localized auroral brightening, however, this brightening was not an auroral breakup. *Kepko et al.* [2004] concluded that some earthward flows occurred up to a few minutes before breakup, however, their estimated time differences between reconnection and breakup are likely within the margin of uncertainty in image data and the definition of the onset times of breakup and flow. For example, they defined the onset time as the time of the first image with brightening, which is different by ~1 min from the definition of the onset time in our study, which adopts the center time between the image with brightening and the previous image.

[62] *Ohtani et al.* [1999] reported a tailward flow that initiated 4 min before substorm onset primarily on the basis of observations of Pi2 geomagnetic pulsation on the ground. *Nagai et al.* [1998] reported an earthward flow initiating 2 min before the detection of Pi2. These flows may have been observed prior to auroral breakup, even taking a possible delay of Pi2 from breakup by 1–3 min [*Liou et al.*, 2000]. The existence of such flow prior to breakup should be confirmed with global images to make sure that there is no preceding pseudo-breakups. *Baker et al.* [2002] concluded that a tailward flow was observed 7 min prior to a breakup in global images. However, they also found several preceding pseudo-breakups. The tailward flow may thus be associated with these pseudo-breakups, rather than with the major breakup.

[63] *Slavin et al.* [2002] showed auroral breakups accompanied by earthward flows/dipolarizations at $X = -9\ R_E$ within ~1 min and by TCRs at $X \sim -30\ R_E$ ~2 min later. They assumed that near-earth reconnection had occurred prior to these earthward flows and TCRs somewhere between them, and estimated that reconnection occurred at $X \sim -15$ to $-18\ R_E$ about 2–5 min prior to breakups. For the same event, however, *Lyons* [2000] concluded that reconnection initiated after breakup, assuming that the detection of TCRs marks the onset time of reconnection. It thus appears that different conclusions regarding the causality between breakup and reconnection currently stems from different assumption on the propagation time of disturbance from NENL to satellites.

[64] In summary, we believe that there is no definitive evidence in the present results or in the literature that reconnection initiates before breakup. While it is possible that reconnection may initiate before breakup, it currently appears more reasonable to conclude that near-earth reconnection occurs simultaneously within a few minutes of breakup on an observational basis.

6. Summary

[65] We have studied tailward flows ($V_x \leq -200$ km/s) with southward magnetic field ($B_z < 0$) in the plasma sheet at $-25 > X_{AGSM} \geq -31\ R_E$ around the times of 66 isolated auroral breakups. Tailward flows were typically observed at $0 \leq Y_{AGSM} < 5\ R_E$, but were also often observed in $-5 \leq Y_{AGSM} < 10\ R_E$ in Figure 4. A clear development of tailward flows was identified at the times of breakup in Figure 5, with tailward flows occurring in 25 of 37 cases (68%) in $-5 \leq Y_{AGSM} < 10\ R_E$. The Y location of relatively fast tailward flow ($V_x \leq -400$ km/s) was found to be closely correlated with breakup MLT (correlation coefficient, 0.8) as obtained in Figure 6, and was represented as $Y_{AGSM} = -5.7 \times (\mathrm{MLT} + 0.6)\ R_E$.

[66] This relationship was interpreted to indicate that tailward flow/reconnection occurs near breakup MLT, by studying the foot point of tailward flows in Figure 7. Tailward flows were shifted dawnward from breakup MLT by 0.3 hour but this displacement was statistically not significant in our data set. Tailward flows have a typical dawn–dusk dimension ~10 R_E in Figure 6 or ~2 hours in MLT in Figure 7.

[67] Inside 5 R_E from the modeled Y_{AGSM} locations, tailward flows occurred in 88% of the 26 cases at the times of breakup between 22 and 0 MLT in Figure 8. The high occurrence rate implies that breakups are invariably accompanied by tailward flows near breakup MLT. Reconnection is usually formed inside 25 R_E down the tail, since tailward flows were almost always observed beyond 25 R_E.

[68] There were two events without tailward flows near the modeled Y location in Figure 6. However, they were an earthward flow (Figure 9) and a TCR in PSBL (Figure 10), which were not inconsistent with reconnection. Auroral breakup is thus likely to always be accompanied by near-earth reconnection near breakup MLT.

[69] Given the time delay for the arrival of tailward flows generated by reconnection to a satellite as a few minutes, reconnection appears to occur simultaneously with breakup within a few minutes. Further measurements to determine the time difference will be required in order to clarify the cause-and-effect relationship between auroral breakup and near-tail reconnection.

[70] **Acknowledgments.** We are grateful to S. Kokubun and T. Nagai for providing the Geotail magnetic field data. The SYM-H index was provided by the World Data Center for Geomagnetism, Kyoto. The OMNI data were obtained from the GSFC/SPDF OMNIWeb interface at http://omniweb.gsfc.nasa.gov. A.I. thanks A. Nishida, L. R. Lyons, T. Nagai, T. Hori, and Y. Ebihara for their valuable comments. This work was partly performed while A.I. held a National Research Council—NASA/GSFC research associateship. This work was supported by Grant-in-Aid for Young Scientists (B) (17740325) from the Ministry of Education, Culture, Sports, Science, and Technology (MEXT), Japan, and by the Grant-in-Aid for Creative Scientific Research "The Basic Study of Space Weather Prediction" (17GS0208, Head Investigator: K. Shibata) from the Ministry of Education, Culture, Sports, Science, and Technology of Japan.

[71] Wolfgang Baumjohann thanks Victor Sergeev and Anatoli Petrukovich for their assistance in evaluating this paper.

References

Akasofu, S.-I. (1964), The development of the auroral substorm, *Planet. Space Sci.*, *12*, 273–282.

Angelopoulos, V., et al. (1997), Magnetotail flow bursts: Association to global magnetospheric circulation, relationship to ionospheric activity and direct evidence for localization, *Geophys. Res. Lett.*, *24*(18), 2271–2274.

Baker, D. N., T. I. Pulkkinen, V. Angelopoulos, W. Baumjohann, and R. L. McPherron (1996), Neutral line model of substorms: Past results and present view, *J. Geophys. Res.*, *101*(A6), 12,975–13,010.

Baker, D. N., et al. (2002), Timing of magnetic reconnection initiation during a global magnetospheric substorm onset, *Geophys. Res. Lett.*, *29*(24), 2190, doi:10.1029/2002GL015539.

Baumjohann, W., M. Hesse, S. Kokubun, T. Mukai, T. Nagai, and A. A. Petrukovich (1999), Substorm dipolarization and recovery, *J. Geophys. Res.*, *104*(A11), 24,995–25,000.

de la Beaujardière, O., L. R. Lyons, J. M. Ruohoniemi, E. Friis-Christensen, C. Danielson, F. J. Rich, and P. T. Newell (1994), Quiet-time intensifications along the poleward auroral boundary near midnight, *J. Geophys. Res.*, *99*(A1), 287–298.

Fillingim, M. O., G. K. Parks, L. J. Chen, M. Brittnacher, G. A. Germany, J. F. Spann, D. Larson, and R. P. Lin (2000), Coincident Polar/UVI and WIND observations of pseudobreakups, *Geophys. Res. Lett.*, *27*(9), 1379–1382.

Frank, L. A., J. B. Sigwarth, W. R. Paterson, and S. Kokubun (2001), Two encounters of the substorm onset region with the Geotail spacecraft, *J. Geophys. Res.*, *106*(A4), 5811–5831.

Galand, M., and D. Lummerzheim (2004), Contribution of proton precipitation to space-based auroral FUV observations, *J. Geophys. Res.*, *109*, A03307, doi:10.1029/2003JA010321.

Germany, G. A., G. K. Parks, M. Brittnacher, J. Cumnock, D. Lummerzheim, J. F. Spann, L. Chen, P. G. Richards, and F. J. Rich (1997), Remote determination of auroral energy characteristics during substorm activity, *Geophys. Res. Lett.*, *24*(8), 995–998.

Germany, G. A., J. F. Spann, G. K. Parks, M. J. Brittnacher, R. Elsen, L. Chen, D. Lummerzheim, and M. H. Rees (1998), Auroral observations from the Polar ultraviolet imager (UVI), in *Geospace Mass and Energy Flow: Results From the International Solar-Terrestrial Physics Program*, *Geophys. Monogr. Ser.*, vol. 104, edited by J. L. Horwitz et al., pp. 149–160, AGU, Washington, D. C.

Germany, G. A., D. Lummerzheim, and P. G. Richards (2001), Impact of model differences on quantitative analysis of FUV auroral emissions: Total ionization cross sections, *J. Geophys. Res.*, *106*(A7), 12,837–12,843.

Hayakawa, H., A. Nishida, E. W. Hones Jr., and S. J. Bame (1982), Statistical characteristics of plasma flow in the magnetotail, *J. Geophys. Res.*, *87*(A1), 277–283.

Ieda, A., S. Machida, T. Mukai, Y. Saito, T. Yamamoto, A. Nishida, T. Terasawa, and S. Kokubun (1998), Statistical analysis of the plasmoid evolution with Geotail observations, *J. Geophys. Res.*, *103*(A3), 4453–4465.

Ieda, A., D. H. Fairfield, T. Mukai, Y. Saito, S. Kokubun, K. Liou, C.-I. Meng, G. K. Parks, and M. J. Brittnacher (2001), Plasmoid ejection and auroral brightenings, *J. Geophys. Res.*, *106*(A3), 3845–3857.

Ieda, A., et al. (2003), Quiet time magnetotail plasma flow: Coordinated Polar ultraviolet images and Geotail observations, *J. Geophys. Res.*, *108*(A9), 1345, doi:10.1029/2002JA009739.

Ieda, A., T. Mukai, S. Machida, J.-H. Shue, S.-I. Ohtani, T. Nagai, and Y. Saito (2004), Difference between earthward and tailward flows in their dependences on geomagnetic and IMF conditions, *COSPAR Colloq. Ser.*, *16*, 186–189.

Iyemori, T. (1990), Storm-time magnetospheric currents inferred from mid-latitude geomagnetic field variations, *J. Geomagn. Geoelectr.*, *42*, 1249–1265.

Kepko, L., M. G. Kivelson, R. L. McPherron, and H. E. Spence (2004), Relative timing of substorm onset phenomena, *J. Geophys. Res.*, *109*, A04203, doi:10.1029/2003JA010285.

King, J. H., and N. E. Papitashvili (2005), Solar wind spatial scales in and comparisons of hourly Wind and ACE plasma and magnetic field data, *J. Geophys. Res.*, *110*, A02104, doi:10.1029/2004JA010649.

Kokubun, S., T. Yamamoto, M. H. Acuña, K. Hayashi, K. Shiokawa, and H. Kawano (1994), The Geotail magnetic field experiment, *J. Geomagn. Geoelectr.*, *46*, 7–21.

Li, L., and R. L. Xu (2000), A neutral sheet surface observed on ISEE-2, IMP-8, AMPTE/IRM, and INTERBALL satellites, *Geophys. Res. Lett.*, *27*(6), 855–858.

Liou, K., C.-I. Meng, P. T. Newell, K. Takahashi, S.-I. Ohtani, A. T. Y. Lui, M. Brittnacher, and G. Parks (2000), Evaluation of low-latitude Pi2 pulsations as indicators of substorm onset using Polar ultraviolet imagery, *J. Geophys. Res.*, *105*(A2), 2495–2505.

Liou, K., P. T. Newell, D. G. Sibeck, C.-I. Meng, M. Brittnacher, and G. Parks (2001), Observation of IMF and seasonal effects in the location of auroral substorm onset, *J. Geophys. Res.*, *106*(A4), 5799–5810.

Lui, A. T. Y. (1996), Current disruption in the earth's magnetosphere: Observations and models, *J. Geophys. Res.*, *101*, 13,067–13,088.

Lui, A. T. Y., K. Liou, P. T. Newell, C.-I. Meng, S.-I. Ohtani, T. Ogino, S. Kokubun, M. J. Brittnacher, and G. K. Parks (1998), Plasma and magnetic flux transport associated with auroral breakups, *Geophys. Res. Lett.*, *25*(21), 4059–4062.

Lummerzheim, D., M. Brittnacher, D. Evans, G. A. Germany, G. K. Parks, M. H. Rees, and J. F. Spann (1997), High time resolution study of the hemispheric power carried by energetic electrons into the ionosphere during the May 19/20, 1996 auroral activity, *Geophys. Res. Lett.*, *24*(8), 987–990.

Lyons, L. R. (2000), Determinations of relative timing of near-earth substorm onset and tail reconnection, in *ESA SP-443*, pp. 255–262, Eur. Space Agency, Noordwijk, Netherlands.

Lyons, L. R., E. Zesta, Y. Xu, E. R. Sanchez, J. C. Samson, G. D. Reeves, J. M. Ruohoniemi, and J. B. Sigwarth (2002), Auroral poleward boundary intensifications and tail bursty flows: A manifestation of a large-scale ULF oscillation?, *J. Geophys. Res.*, *107*(A11), 1352, doi:10.1029/2001JA000242.

Machida, S., Y. Miyashita, A. Ieda, A. Nishida, T. Mukai, Y. Saito, and S. Kokubun (1999), Geotail observations of flow velocity and north–south magnetic field variations in the near and mid-distant tail associated with substorm onsets, *Geophys. Res. Lett.*, *26*(6), 635–638.

Machida, S., A. Ieda, T. Mukai, Y. Saito, and A. Nishida (2000), Statistical visualization of earth's magnetotail during substorms by means of multidimensional superposed epoch analysis with Geotail data, *J. Geophys. Res.*, *105*(A11), 25,291–25,303.

Macmillan, S., and S. Maus (2005), International geomagnetic reference field—The tenth generation, *Earth Planets Space*, *57*, 1135–1140.

Miyashita, Y., S. Machida, K. Liou, T. Mukai, Y. Saito, H. Hayakawa, C.-I. Meng, and G. K. Parks (2003), Evolution of the magnetotail associated with substorm auroral breakups, *J. Geophys. Res.*, *108*(A9), 1353, doi:10.1029/2003JA009939.

Moldwin, M. B., and W. J. Hughes (1993), Geomagnetic substorm association of plasmoids, *J. Geophys. Res.*, *98*(A1), 81–88.

Mukai, T., S. Machida, Y. Saito, M. Hirahara, T. Terasawa, N. Kaya, T. Obara, M. Ejiri, and A. Nishida (1994), The low energy particle (LEP) experiment onboard the Geotail satellite, *J. Geomagn. Geoelectr.*, *46*, 669–692.

Nagai, T., K. Takahashi, H. Kawano, T. Yamamoto, S. Kokubun, and A. Nishida (1994), Initial Geotail survey of magnetic substorm signatures in the magnetotail, *Geophys. Res. Lett.*, *21*(25), 2991–2994.

Nagai, T., M. Fujimoto, Y. Saito, S. Machida, T. Terasawa, R. Nakamura, T. Yamamoto, T. Mukai, A. Nishida, and S. Kokubun (1998), Structure and dynamics of magnetic reconnection for substorm onsets with Geotail observations, *Geophys. Res. Lett.*, *103*(A3), 4419–4440.

Nakamura, R., W. Baumjohann, M. Brittnacher, V. A. Sergeev, M. Kubyshkina, T. Mukai, and K. Liou (2001a), Flow bursts and auroral activations: Onset timing and foot point location, *J. Geophys. Res.*, *106*(A6), 10,777–10,789.

Nakamura, R., W. Baumjohann, R. Schödel, M. Brittnacher, V. A. Sergeev, M. Kubyshkina, T. Mukai, and K. Liou (2001b), Earthward flow bursts, auroral streamers and small expansions, *J. Geophys. Res.*, *106*(A6), 10,791–10,802.

Nishida, A., H. Hayakawa, and E. W. Hones Jr. (1981), Observed signatures of reconnection in the magnetotail, *J. Geophys. Res.*, *86*(A3), 1422–1436.

Nishida, A., T. Mukai, T. Yamamoto, Y. Saito, and S. Kokubun (1996), Magnetotail convection in geomagnetically active times: 1. Distance to the neutral lines, *J. Geomagn. Geoelectr.*, *48*, 489–501.

Ohtani, S., F. Creutzberg, T. Mukai, H. Singer, A. T. Y. Lui, M. Nakamura, P. Prikryl, K. Yumoto, and G. Rostoker (1999), Substorm onset timing: The December 31, 1 995, event, *J. Geophys. Res.*, *104*(A10), 22,713–22,727.

Ohtani, S., R. Yamaguchi, M. Nosé, H. Kawano, M. Engebretson, and K. Yumoto (2002), Quiet time magnetotail dynamics and their implications for the substorm trigger, *J. Geophys. Res.*, *107*(A2), 1030, doi:10.1029/2001JA000116.

Owen, C. J., and J. A. Slavin (1992), Energetic ion events associated with traveling compression regions, in *ESA SP-335*, pp. 365–370, Eur. Space Agency, Paris, France.

Pulkkinen, T. I., et al. (1998), Two substorm intensifications compared: Onset, expansion, and global consequences, *J. Geophys. Res.*, *103*(A1), 15–27.

Richmond, A. D. (1995), Ionospheric electrodynamics using magnetic apex coordinates, *J. Geomagn. Geoelectr.*, *47*, 191–212.

Rostoker, G. (1998), On the place of the pseudo-breakup in a magnetospheric substorm, *Geophys. Res. Lett.*, *25*(2), 217–220.

Shiokawa, K., et al. (1998), High-speed ion flow, substorm current wedge, and multiple Pi2 pulsations, *J. Geophys. Res.*, *103*(A3), 4491–4507.

Shue, J.-H., S. Ohtani, P. T. Newell, K. Liou, C.-I. Meng, A. Ieda, and T. Mukai (2003), Quantitative relationships between plasma sheet fast flows and nightside auroral power, *J. Geophys. Res.*, *108*(A6), 1231, doi:10.1029/2002JA009794.

Slavin, J. A., E. J. Smith, D. G. Sibeck, D. N. Baker, R. D. Zwickl, and S. I. Akasofu (1985), An ISEE 3 study of average and substorm conditions in the distant magnetotail, *J. Geophys. Res.*, *90*(A11), 10,875–10,895.

Slavin, J. A., M. F. Smith, E. L. Mazur, D. N. Baker, E. W. Hones Jr., T. Iyemori, and E. W. Greenstadt (1993), ISEE 3 observations of traveling compression regions in the earth's magnetotail, *J. Geophys. Res.*, *98*(A9), 15,425–15,446.

Slavin, J. A., et al. (2002), Simultaneous observations of earthward flow bursts and plasmoid ejection during magnetospheric substorms, *J. Geophys. Res.*, *107*(A7), 1106, doi:10.1029/2000JA003501.

Taguchi, S., J. A. Slavin, and R. P. Lepping (1998), Traveling compression regions in the midtail: Fifteen years of IMP 8 observations, *J. Geophys. Res.*, *103*(A8), 17,641–17,650.

Torr, M., et al. (1995), A far ultraviolet imager for the international solar-terrestrial physics mission, *Space Sci. Rev.*, *71*, 329–383.

Tsyganenko, N. A., and D. P. Stern (1996), Modeling the global magnetic field of the large-scale Birkeland current systems, *J. Geophys. Res.*, *101*(A12), 27,187–27,198.

D. H. Fairfield and J. A. Slavin, Heliophysics Science Division, NASA Goddard Space Flight Center, Greenbelt, MD 20771, USA.

M. O. Fillingim and G. K. Parks, Space Sciences Laboratory, University of California, 7 Gauss Way, Berkeley, CA 94720, USA.

A. Ieda, Solar-Terrestrial Environment Laboratory, Nagoya University, Furo-cho, Chikusa-ku, Nagoya, Aichi 464-8601, Japan. (ieda@stelab.nagoya-u.ac.jp)

K. Liou and C.-I. Meng, Applied Physics Laboratory, Johns Hopkins University, 11100 John Hopkins Road, Laurel, MD 20723, USA.

S. Machida, Department of Geophysics, Kyoto University, Oiwake-cho, Kitashirakawa, Sakyo-ku, Kyoto 606-8502, Japan.

Y. Miyashita, T. Mukai, and Y. Saito, Institute of Space and Astronautical Science, Japan Aerospace Exploration Agency, 3-1-1 Yoshinodai, Sagamihara, Kanagawa 229-8510, Japan.

M. Nosé, Data Analysis Center for Geomagnetism and Space Magnetism, Graduate School of Science, Kyoto University, Oiwake-cho, Kitashirakawa, Sakyo-ku, Kyoto 606-8502, Japan.

J.-H. Shue, Institute of Space Science, National Central University, Jhongli City, Taoyuan County 32001, Taiwan.